scientific reports

OPEN

Microstructure and properties of joint of Al/Cu welded by resistance element welding with an auxiliary gasket of Ni

Dongsheng Cui[1,2], Jing Wang[1], Ranfeng Qiu[1,3✉], Hongxin Shi[1,2] & Lipeng Yan[4]

A rivet of aluminum and auxiliary gasket of nickel were adopted to weld A1060 aluminum plate and T2 copper plate using resistance element welding. The interfacial microstructure was analyzed and the tensile shear load of the joint was tested. A layer of Al_2Cu and the eutectic structure of Al_2Cu and (Al) were formed in the interfacial zone of Al/Cu. The grains in Al_2Cu layer exhibit random crystal orientations. With the increase of welding current and the extension of welding time, the tensile shear load of the Al/Cu joint increased first and then decreased. When the welding current was 30 kA, the welding time was 400 ms, the tensile shear load of the joint reached the maximum, approximately 2.55 kN. The results reveal that the application of nickel auxiliary gasket in the resistance element welding of Al/Cu can promote the joining between the rivet shank and the upper plate and increase the tensile shear load of the joint.

Keywords Resistance element welding, Aluminum, Copper, Microstructure, Performance

In recent years, new energy vehicles have developed rapidly in the background of saving energy, protecting the natural environment and reducing the emission of CO_2[1,2]. Different from conventional fuel car, new energy vehicles use batteries as the power source. Copper are widely used because of their excellent electrical conductivity[3]. However, copper is not only expensive, but also dense. Hence, people begin to focus on aluminum, which also has excellent electrical conductivity only lower than silver and copper[4]. In the new energy vehicles, replacing copper with aluminum can reduce the weight of the vehicle, and then improve the endurance. However, some factors such as structure, economy, and electrical conductivity need to be considered in the process of selecting aluminum or copper. In the case of space permitting, aluminum with lower density should be preferred, while copper with more outstanding overcurrent capacity should be chosen in other extreme conditions. In view of this, the joining of aluminum and copper is an essential challenge in the electrical system.

When aluminum and copper are welded by conventional fusion welding, the size of grains in heat affected zone may be coarse due to immense heat input, and massive intermetallic compounds (IMCs) can be formed in the interface of Al/Cu[5]. To improved the above issues, the high energy density welding methods, such as electron beam welding[6–8] and laser welding[9,10] were utilized to weld Al/Cu. In addition, other solid-state welding methods with low welding temperature, such as friction stir welding[11,12] and ultrasonic welding[13,14], were also selected to weld Al/Cu. However, there is no perfect welding method, and each welding method has its limitations in a particular application. Comparing to the above methods, resistance spot welding (RSW) is an appropriate method, which suits for welding the thin plates[15]. RSW is a method of placing the welded sheets between the upper and lower electrodes, pressurizing and energizing them, and using the generated resistance heat to melt the welded metal to achieve joining. In fact, the busbars made of aluminum and copper in the batteries happens to be a thin plate structure. Undoubtedly, using RSW to join busbars made of aluminum and copper is considered appropriate.

Nevertheless, there are two challenging subjects. One is that a large amount of IMCs formed at the interface between aluminum and copper, which possesses an adverse influence on the performance of the joint, and the other is that reliable joint of Al/Cu are considered difficult to achieve due to the their splendid electrical

[1]School of Materials Science and Engineering, Henan University of Science and Technology, Luoyang 471039, China. [2]Provincial and Ministerial Co-Construction of Collaborative Innovation Center for Nonferrous Metal New Materials and Advanced Processing Technology, Luoyang 471039, China. [3]Science and Technology Innovation Center of Intelligent Equipment & Advanced Materials, Longmen Laboratory, Luoyang 471039, China. [4]College of Material Science and Engineering, Henan Institute of Technology, Xinxiang 453003, China. ✉email: qiurf1221@163.com

and thermal conductivity. Based on RSW, an advanced technology named resistance element welding (REW), which is suitable for the joining of dissimilar materials has been developed. Up to now, REW has successfully applied to weld aluminum/steel[16–18], magnesium/steel[19], aluminum/titanium[20], aluminum/magnesium[21] and other dissimilar metal system. Through changing the shape of rivet can achieve the one-step REW without prefabricated hole in base metal, and that is why the technology is considered as an extremely promising method for joining dissimilar metals. So far, there are few reports about using REW to weld Al/Cu. In response to this, A1060 pure aluminum and T2 pure copper were welded using the welding technology in this study. For the REW of dissimilar materials, the joining between the rivet shank and the lower plate, between the rivet shank and the upper plate are important roles to form a solid joint. The former is the guarantee of the bearing capacity of the joint, and the latter prevents the upper plate from rotating around the rivet shank. However, when REW of Al/Cu is implemented, the joining between the rivet shank and the upper plate is difficult to achieve due to the better thermal conductivity of the upper plate (copper). Therefore, the Ni sheet was selected as an auxiliary gasket (AG) in this study, which was placed between the upper plate and the rivet cap during welding. The purpose of inserting AG is to generate more heat during the welding process. There are two reasons why Ni sheet was selected as AG in this study. First, nickel has a higher resistivity compared with copper and aluminum. Second, no additional metal impurities are introduced into the circuit system, because the copper busbars used in the circuit are also often nickel-coated. In this study, the microstructure and performance of the joint welded by REW with an AG were analyzed.

Experimental materials and procedures
Experimental materials
In this study, 2 mm thick commercial A1060 pure aluminum and T2 pure copper plate was used as lower plate and upper plate (they are the materials to be welded and are called base materials), respectively. An A1060 pure aluminum rivet, which is a third insert in the joint for joining the upper and lower plates, was selected as an element. A pure nickel sheet in the shape of 30 mm × 30 mm × 0.8 mm was used as an AG. Here, the AG is a gasket used for auxiliary welding, its role is to increase the heat generated during the welding process. Figure 1a shows the making process of the sample. First, the rivet and AG were machined according to the dimensions shown in Fig. 1a. Here, the length of the rivet shank (2.8 mm) is consistent with the thickness of both the upper plate and the AG. A hole with a diameter of 6 mm was prefabricated at the center of the AG. The distance between the center of the hole and the edge of the AG was 15 mm. Second, the upper and lower plates were cut to 100 mm × 30 mm shape. A hole with a diameter of 6 mm was also prefabricated at the center of the upper plate (copper plate) as shown in Fig. 1a.

Welding process
Figure 1b shows the assembly and welding process of the sample. Firstly, the upper plate, lower plate, rivet and AG were cleaned using alcohol before welding, then air-dried. Secondly, they were assembled as shown in Fig. 1b. The AG was palced between the rivet cap and the upper plate, and then the rivet shank was fit into the holes of the AG and upper plate. Thirdly, the assembled sample was placed between the upper and lower electrodes of the RSW machine and the rivet cap was on one side of the upper electrode. Fourthly, aligned the upper and lower electrodes with the rivet, and turned on the RSW machine switch and started welding. Welding current (WC) varied from 29 to 31 kA with an interval of 0.5 kA when welding time (WT) and electrode pressure remain unchanged at 400 ms and 3.1 kN, respectively. The WT varied within the range of 200–600 ms with an interval of 100 ms when the fixed WC was 300 kA and the electrode pressure was 3.1 kN.

Performance testing and microstructure analysis
After welding, the tensile shear load of the joints was tested using the tensile testing machine at room temperature, and the speed maintained 1 mm/s. The specimens for microstructural observations were prepared by cutting through the center of the joint along the direction of perpendicular to the lap interface using the wire cutting machine, and then the cross section was ground and polished. The microstructure of the interface was observed
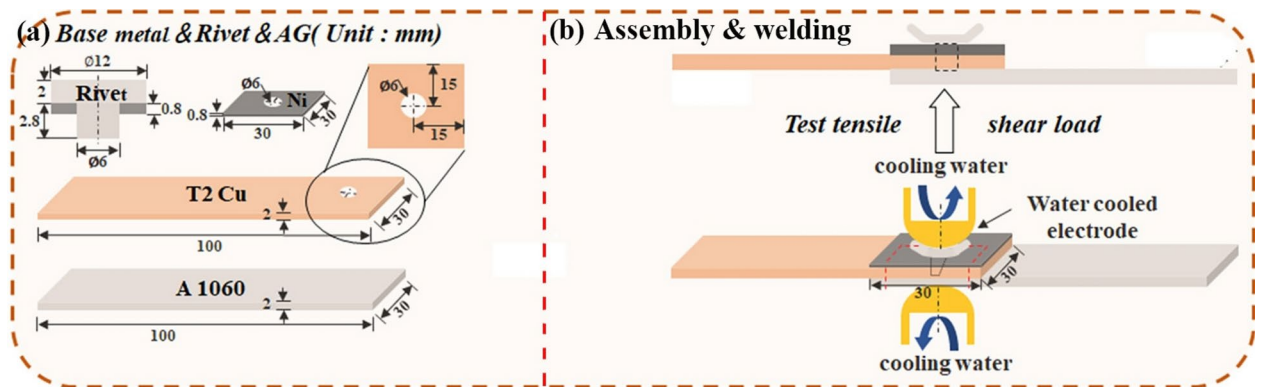

Fig. 1. Schematic diagram of making process of the sample (**a**) and assembly and welding process (**b**).
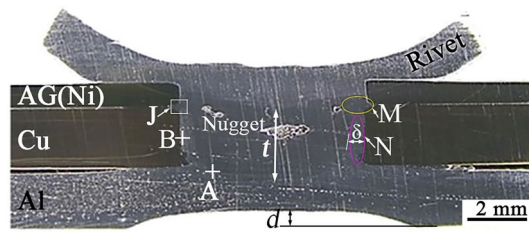
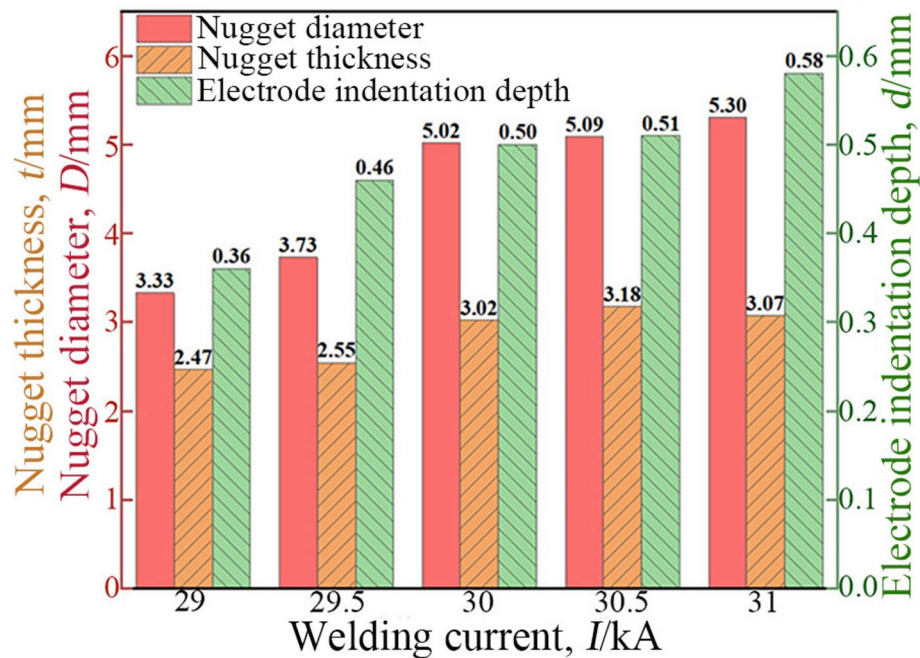**Fig. 2**. Cross section of the Al/Cu joint.

Fig. 3. Effect of WC on size of joint cross section.

using the scanning electron microscopy (SEM) with energy dispersive X-ray spectroscopy (EDS). The specimen for electron backscatter diffraction (EBSD) was prepared by polishing with argon ions after mechanical polishing.

Results and discussion

Figure 2 shows a typical cross section of the joint between A1060 pure aluminum and T2 pure copper welded by REW (hereafter known as Al/Cu joint). The joint was welded at the WC of 30 kA and WT of 400 ms. A nugget was observed in Fig. 2. The lower plate and rivet shank were welded together by means of the nugget. From the viewpoint of geometry, the upper part of the nugget was wider and its lower part was narrower. It is thought that AG altered the heat distribution in the welding zone. From the electrode indentation on the surfaces of the joint, it can be seen that the diameter of contact area between the electrode tip and the joint was larger than that of the rivet shank. This shows that the WC flowed not only through the rivet shank but also through the metal around it to the lower plate. Because the resistivity of nickel (20 °C, 6.84×10^{-8} Ω·m) is higher than that of copper (20 °C, 1.68×10^{-8} Ω·m) and aluminum (20 °C, 2.65×10^{-8} Ω·m), more heat was generated at the AG during welding. This caused the rivet shank with lower melting point near the AG to melt, and the zone (M region in Fig. 2) became part of the nugget after solidification. In region farther from AG (N region in Fig. 2), there was a region of width δ between the nugget and the interface of Al/Cu where no melting occurred during welding. Even so, a tight joining was achieved between the rivet shank and the upper plate as shown in Fig. 2. Therefore, the upper part of the nugget was wider and its lower part was narrower.

The nugget diameter of the Al/Cu joint welded under different WC was different. Figure 3 demonstrates the effect of WC on the nugget diameter. Here, the nugget diameter was measured at 1/2 of the thickness of the upper plate on the cross section of the Al/Cu joint. As shown in Fig. 3, the nugget diameter increased with the increase of WC. The greater the WC, the more heat was generated, so that more metal was melted and a larger nugget was formed. However, when the nugget grew to a certain extent, the distance to the upper plate was relatively close. In this case, the heat loss along the upper plate was also increased. This resulted in a more gentle increase in the nugget diameter when the WC was greater than 30 kA. For similar reasons, the nugget thickness

(*t*) also increased with the increase of the WC in the WC range of 29 kA–30.5 k as shown in Fig. 3. However, the nugget thickness of the Al/Cu joint decreased slightly when the WC increased from 30.5 kA to 31kA. This is considered to be due to plastic deformation in the welding zone. The larger the nugget formed, the smaller the supporting force of the welding zone on the electrodes during welding. Under the action of electrode pressure, the welding zone produced plastic deformation, which also thinned the nugget to a certain extent.

As shown in Fig. 2, electrode indentation remained on the surface of both sides of the Al/Cu joint. Figure 3 also demonstrates the effect of WC on the electrode indentation depth of Al/Cu joint. Here, the electrode indentation depth (*t*) was measured on the lower plate side of the Al/Cu joint. The electrode indentation depth increased with the increase of the WC. When the WC was cut off, plastic deformation occurred in the welding zone of the Al/Cu joint under the action of electrode pressure. The larger the nugget formed, the smaller the resistance of the welding zone to plastic deformation. Therefore, the electrode indentation depth increased with the increase of the WC.

Additionally, several pores were observed in the nugget. These pores were inferred to be shrinkage pores according to their shape and location. The reason for the formation of the shrinkage pores is similar to those reported in literature[22].

Figure 4a demonstrates a grain orientation distribution mapping in the boundary region of the nugget, which was detected at the location of A in Fig. 2. According to the morphology of the grains, the nugget was divided into columnar grain zone and equiaxed grain zone. The columnar grain zone was at the outer edge of the nugget, and its width was about 300 μm. The axial direction of these columnar crystals was approximately perpendicular to the outline of the nugget, that is, parallel to the heat dissipation direction during the welding process. These columnar crystals were relatively larger, whereas the average size of equiaxed crystals in the nugget was about 38.23 μm. In addition, the grains in the rivet shank and lower plate regions outside the nugget were equiaxed, with average sizes of 34.45 μm and 25.54 μm, respectively.

Figure 4b shows grain boundaries misorientation angle distribution in the boundary region of the nugget. The results of statistical analysis show that low angle boundaries (LABs, the grain boundaries misorientation angle is 2°–15°) and high angle boundaries (HABs, the grain boundaries misorientation angle is greater than 15°) account for 37.2% and 62.8% in the region, respectively. LABs were mainly distributed in the rivet shank region outside the nugget, while the grains in the nugget were mainly HABs. The reason is considered to be that rivet was made by extrusion, and the nugget was formed after the metal was melted and solidified where the original pressure processing organizational characteristics were eliminated. Figure 4c represented the histograms of boundary misorientation distributions. This region was characterized by a high proportion of
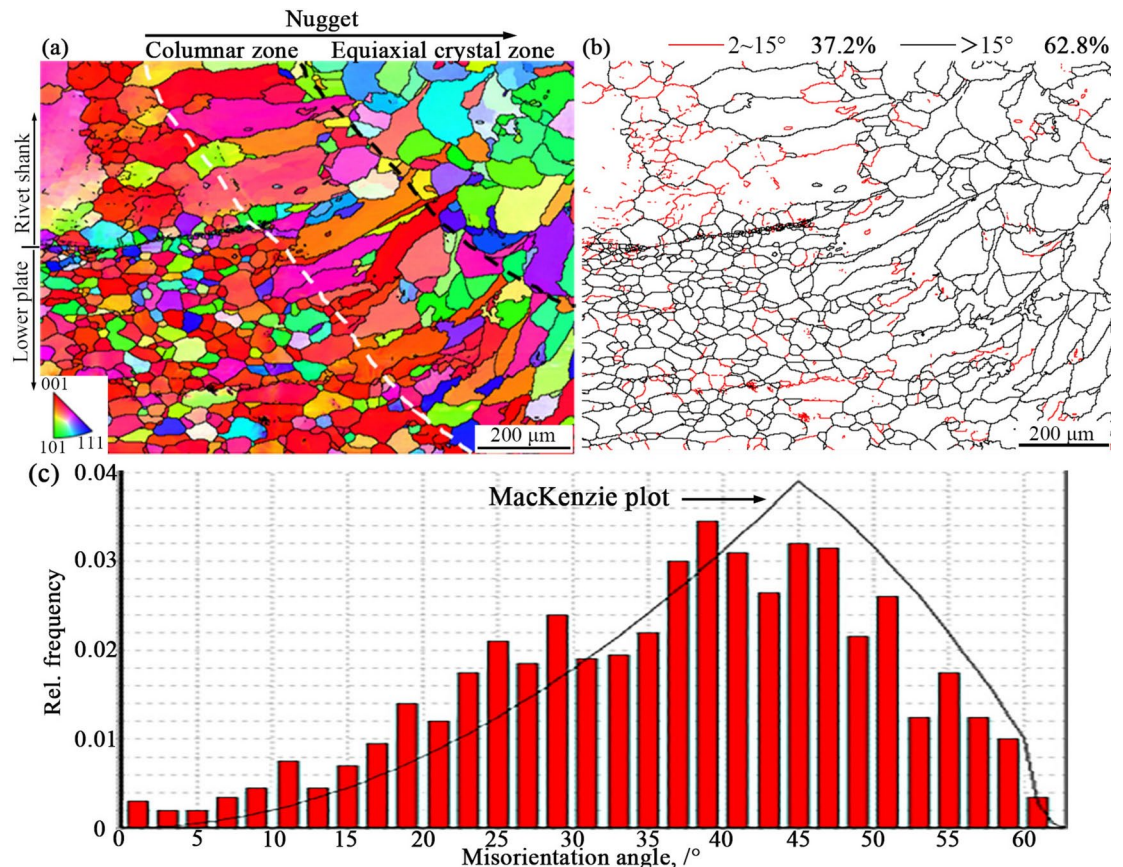

Fig. 4. Grain orientation distribution (**a**); grain boundaries misorientation angle distribution (**b**); histograms of boundary misorientation distributions (**c**).

HABs. The distribution of the boundary misorientation matched the MacKenzie plot, indicated that dynamic recrystallization taken place in this region.

As shown in Fig. 4a, the columnar crystals had obvious preference orientation, and the grains grew approximately along the <100> direction. When the liquid metal in the nugget solidified, heterogeneous nucleation occurred attached to the surrounding solid wall. In the formed grains, those grains, whose easiest direction to grow was consistent with the fastest heat dissipation direction, grew preferentially and into coarse columnar crystals. With the solidification, the grain nucleation and growth conditions at the front of the solid–liquid interface changed. The concentration of solute as nucleation particle increased, which provided favorable conditions for crystallization nucleation. The direction of heat dissipation tended to be isotropic. Therefore, equiaxed crystals without preferred orientation were formed in the central region of the nugget, and coarse columnar crystals with preferred orientation were formed in the outer region of the nugget.

Figure 5a shows a SEM image of vertical interface of the AG-upper plate and the rivet shank, which was taken from location B in Fig. 2. An "n" shaped melting mark was observed in the aluminum (rivet shank). A banded melting layer was formed in the aluminum adjacent to the copper (upper plate), and the interfacial remelting zone (IRZ) was formed after solidification. In the direction of plate thickness, the length of the IRZ was approximately the same as the upper plate thickness. As mentioned above, the M zone was formed in the rivet shank near of the lower half of the AG, which was also formed after melting and solidification during welding. As shown in Fig. 5a, the IRZ and the nugget were connected through the M zone. In addition, a layer of metal (later called interstitial layer) was observed in the gap between the upper plate and the AG plate. Under the action of electrode pressure, the expanded liquid metal was squeezed into the gap and solidified to form the interstitial layer.

Figure 5b shows a SEM image of interface between the rivet shank and AG, which was taken from location C in Fig. 5a. No obvious IMCs can be observed at the interface, while some light gray precipitates were observed in the Al (rivet shank) near the interface as shown in Fig. 5b. The composition of the black matrix (A_4 location) and the precipitate (B_4 location) was analyzed and the results are shown in Table 1. Based on the EDS results, it
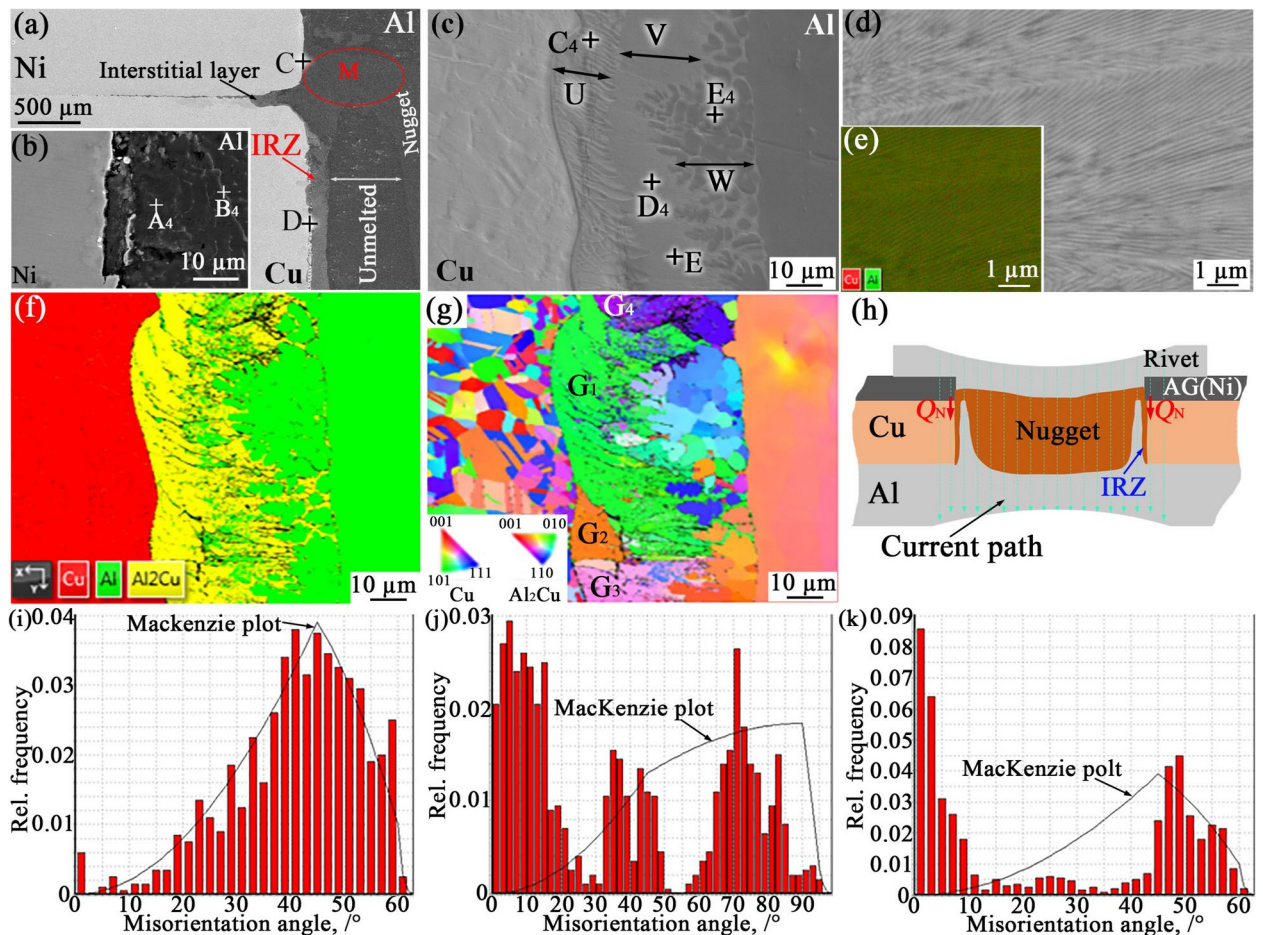

Fig. 5. Microstructure of vertical interface zone and schematic diagram of cross section (**a**) vertical interface; (**b**) SEM image at interface of AG/rivet shank; (**c**) enlarged SEM image of Al/Cu interface; (**d**) high-magnification SEM image of V layer; (**e**) EDS layered image of V layer; (**f**) phase distribution mapping; (**g**) grain orientation distribution; (**h**) schematic diagram of cross section; (**j**), (**i**) and (**k**) histograms of boundary misorientation distributions of Cu, Al_2Cu and Al, respectively.

can be inferred that the black matrix was Al base solid solution (denoted as (Al)), which contains small amounts of Ni and Cu, and that the precipitates was eutectic structure of (Al) and Al_2Cu. From the shape of the AG and the Ni content in (Al) near the interface of Ni/Al, it may be inferred that the AG did not melt during the welding. But, the aluminum in the M zone was melted during the welding as mentioned above. The Ni dissolved into the liquid aluminum during welding, meanwhile, the Cu also spread from other regions to here as described below. During cooling and solidification, the primary phase (Al) was first precipitated here due to the high content of Al in the liquid metal, which was accompanied with that the solute atoms were expelled its surroundings. When cooled to approximately 548 °C, the eutectic structure of (Al) and Al_2Cu was formed where the solute concentration was high.

Figure 5c is an enlarged SEM image at D in Fig. 5a, where the phase distribution mapping is shown in Fig. 5f. According to the morphology presented, the reactants formed in the interface region between the rivet shank and upper plate was divided into three layers U, V and W. Component analysis was performed at local location (C_4, D_4 and E_4) in the three layers, and the results are shown in Table 1. A certain amount of Cu was detected in the both U and V layers, while Al was mainly detected in the W layer. As shown in Fig. 5f, the U layer was mainly composed of Al_2Cu and a small amount of Al, while the W layer was mainly composed of Al and a small amount of Al_2Cu. The EBSD results show that the V layer was also composed of Al_2Cu and Al, although the V layer was suspected to be composed of a single homogeneous phase as shown in Fig. 5c. Figure 5d,e show a high-magnification SEM image and EDS layered image at the E location in Fig. 5c, respectively. It can be seen that layer V was composed of dense two-phase alternating lamellar structure. The analysis results obtained by using EBSD data processing software AZtecCrystal reveal that the proportion of Al_2Cu phase in the U, V, and W layers was 90.6%, 60.2% and 11.7%, respectively. Figure 5g demonstrates a grain orientation distribution mapping corresponding to the field presented in Fig. 5c. The grains in the V and W layers were relatively small, and their size were in the range of 0.6–5.3 μm. They also have no obvious preference orientation. In the U layer, a larger grain (G_1) was detected, which grew approximately along the < 010 > direction as shown in Fig. 5g. However, other Al_2Cu grains (G_2, G_3 and G_4) exhibit a diverse range of colors as depicted in Fig. 5g, suggesting a significantly random orientation of the Al_2Cu grain formed at the interface between the upper plate and the rivet shank.

The reason for the formation of the described above characteristic microstructure in the interfacial region between the rivet shank and upper plate is considered to be the changes in heat distribution resulted from insertion of AG during the welding. Based on the above results, the cross section of the Al/Cu joint can be drawn as shown in Fig. 5h. When the current was switched on for heating, the WC flowed through the rivet shank and its surrounding metal to the lower plate as illustrated in Fig. 5h. The heat generated not only melted part of the rivet shank and the lower plate in the welding center region, but also melted part of the rivet shank adjacent to the interface between the rivet shank and upper plate. The former is a common phenomenon in RSW, which solidified to form the nugget. The achievement of the latter was inseparable from the role of the AG. More heat was generated at the AG during welding due to its high resistivity. The heat (Q_N) not only caused the aluminum near the AG to melt (region M in Fig. 5a), but also conducted to the interface between the rivet shank and upper plate as indicated by the red arrows in Fig. 5h. There were three parts of heat heating the interface between the rivet shank and upper plate: heat transmitted from the nugget and the AG, and resistance heat generated at the region itself. Consequently, the aluminum adjacent to the interface melted to form the IRZ as illustrated in Fig. 5h. Because some of the heat was transmitted outward along the upper plate and lost, the IRZ was narrower as shown in Fig. 5a. When the aluminum near the interface between the rivet shank and upper plate melted, the copper adjacent to it also dissolved. This reduced the liquidus temperature of the mixed liquid metal, which in turn promoted the widening of the IRZ.

Because of the higher copper content there, the primary phase Al_2Cu was first precipitated during cooling in the liquid metal adjacent to the AG. The crystals of primary phase Al_2Cu grew in strips along parallel heat flow direction, which indicates they had the characteristics of faceted growth[22]. Therefore, they also have a certain preference orientation. Subsequently, the eutectic structure of (Al) and Al_2Cu was formed between the lamellar primary strips. The U layer was formed in the interfacial region. On the other side of the IRZ, the primary phase (Al) was precipitated due to the low copper content in the liquid metal, and then the eutectic structure of (Al) and Al_2Cu was formed around them. In this way, the W layer was simultaneously formed in the interfacial region. Since the composition of the liquid metal between the U layer and the W layer was close to the composition at the eutectic point, the liquid–solid coexistence temperature range was very small. Therefore, the eutectic transformation occurs with the decrease of temperature, and the two phases of (Al) and Al_2Cu were coupled with each other to growth and formed the dense lamellar eutectic structure (V layer) due to the faster cooling rate.

Figure 5i–k represent the histograms of boundary misorientation distributions of Cu, Al_2Cu and Al, respectively. The copper plate contained a higher frequency of HABs, but the misorientation distribution of Al_2Cu distributed at almost in every angle. Additionally, it is concluded that the grain misorientation distribution of the

	A_4	B_4	C_4	D_4	E_4	A_9	B_9
Al	99.86	79.18	65.59	80.94	98.80	99.96	99.90
Cu	0.08	20.11	34.41	19.06	1.20	0.04	0.10
Ni	0.08	0.71	0.00	0.00	0.00	0.00	0.00

Table 1. EDS results (at. %).

aluminum plate mainly concentrated in 2–10° and 45–60° from Fig. 5k. In Fig. 5j,k, the boundary misorientation were not correspond to the MacKenzie plot, indicating that full recrystallization has not occured in the zone.

In summary, the zone (J zone in Fig. 2) where the AG, the upper plate and the rivet shank meet played an important role in the formation of the joint. Figure 6a–c demonstrate the SEM image, phase distribution mapping and grain orientation distribution at the J zone shown in Fig. 2, respectively. As shown, the Al_2Cu layer was observed in the Al/Cu interface zone. Near the Al/Ni interface, no IMCs were observed in aluminum, whereas a layer (F location) formation was observed on the Ni side. The results of composition analysis show that the F layer was the solid solution of Al in Ni. Because the solid solubility of Al in solid Ni is larger and the diffusion rate is smaller compared with that in solid Cu, the Al atoms diffused into Ni gathered near the interface and cooled to form the solid solution layer. In addition, Al grains have no obvious preferred orientation in the region, but the grains in the interstitial layer were relatively small, with an average grain size of about 14 μm as shown in Fig. 6c. This is because the interstitial layer was thin and the liquid retention time was short. Figure 6d is an enlarged SEM image at G in Fig. 6a, where phase distribution mapping and grain orientation distribution are shown in Fig. 6e,f. As shown, the structure of the interface region here was similar to one of Al/Cu interface mentioned above, and was also composed of Al_2Cu and the eutectic structure of Al_2Cu and (Al). Here, the Al_2Cu grains also exhibit random crystal orientations.

The formation of the interface structure may be illustrated with illustrations as shown in Fig. 6g–i. Resistance heat was generated in the zone through which the current flows during welding. In addition, the region near the Al/Cu interface was also heated by the heat transmitted from the AG and welding center zone as illustrated in Fig. 6g. As a result, the "n" shaped melting zone was formed in the aluminum near the Al/Cu interface. Meanwhile, some liquid metal was squeezed into the gap between the AG and the upper plate. In the meantime, solid Cu and Ni dissolved into the liquid aluminum, and Al atoms diffused into solid Cu and Ni as illustrated in Fig. 6h. Compared with Cu, Ni with a stronger metal bond was hard to dissolve into liquid aluminum. Hence, the amount of Ni in liquid metals was low. The Cu atoms entering the liquid phase diffused outward from the interface, which was why Cu was detected in the M zone near the AG. During cooling and solidification, the primary phase Al_2Cu was precipitated in the Cu-rich region near the Al/Cu interface, and the (Al) was firstly precipitated in the region with lower Cu content as illustrated in Fig. 6i. Subsequently, the eutectic transformation occurred and the eutectic structure of (Al) and Al_2Cu was formed when cooled to approximately 548 °C.

Figure 7 reveals the effect of WC and WT on the tensile shear load of the Al/Cu joint. With the increase of WC and the extension of WT, the tensile shear load of the Al/Cu joint increased first and then decreased. When the WC was 30 kA, the WT was 400 ms, the tensile shear load of the joint reached the maximum, approximately
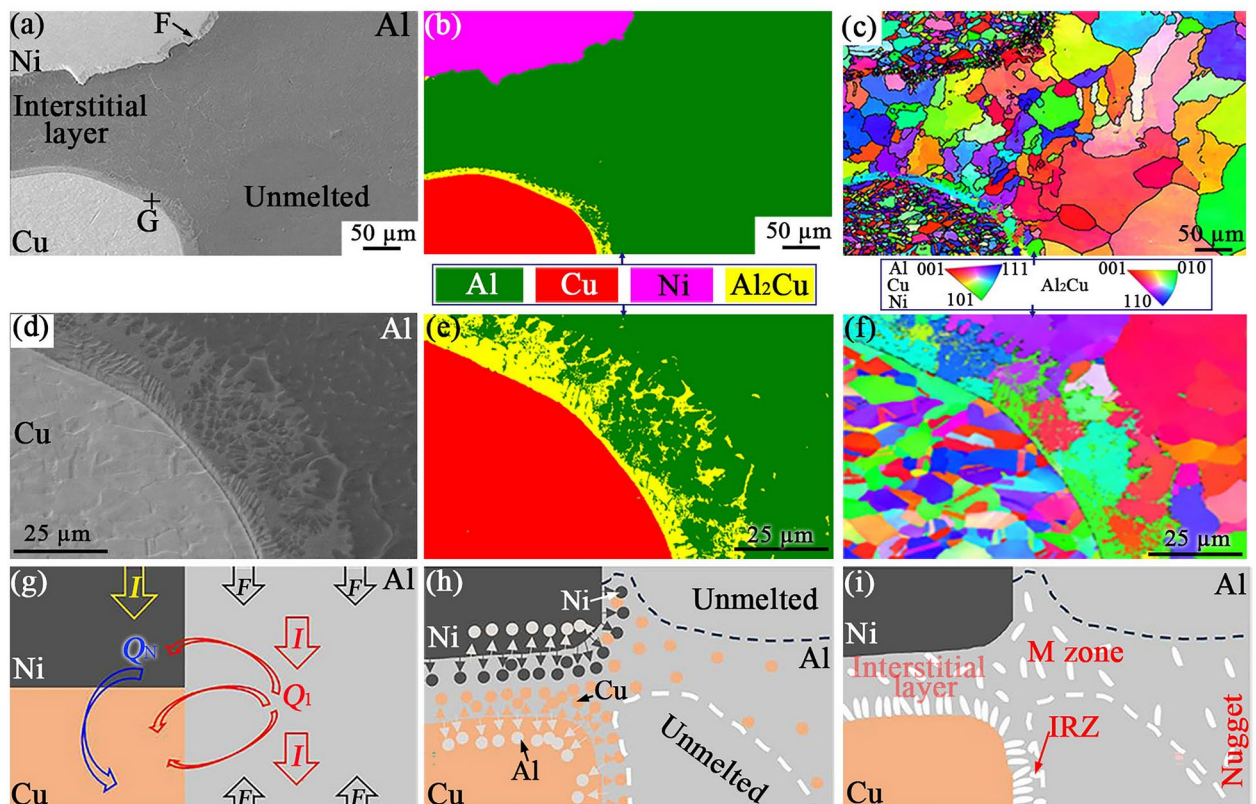

Fig. 6. Images and schematic diagram of atomic diffusion at J zone in Fig. 2 (**a**), (**b**) and (**c**) SEM image, phase distribution mapping and grain orientation distribution at the J zone, respectively; (**d**), (**e**) and (**f**) SEM image, phase distribution mapping and grain orientation distribution at the G location, respectively; (**g**), (**h**) and (**i**) schematic diagram of atomic diffusion.
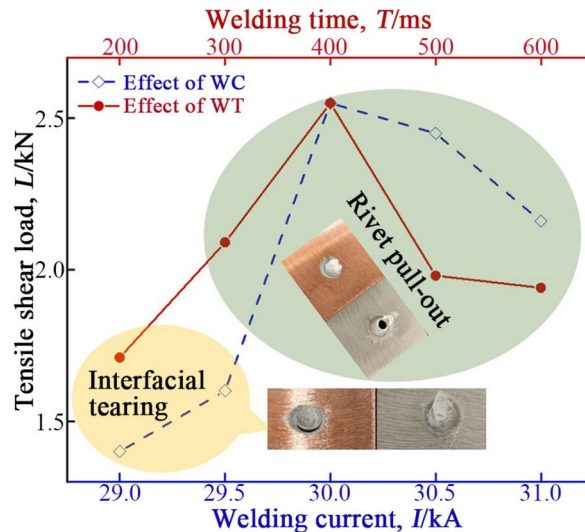
Fig. 7. Effect of WC and WT on the tensile shear load of the Al/Cu joint.
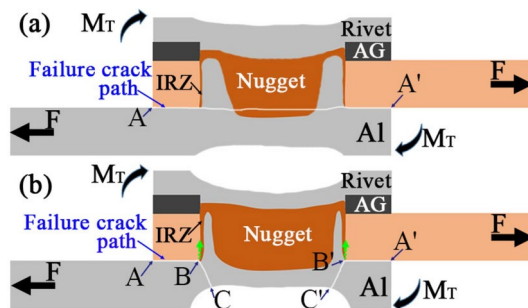

Fig. 8. Fracture diagram of the joint (**a**) interfacial tearing; (**b**) rivet pull-out.

2.55 kN. In this study, there were two modes of Al/Cu joint failure: interface tearing and rivet pull-out. The Al/Cu joint presented the interface tearing failure mode when the WC was lower than 29.5 kA, while the failure mode of the Al/Cu joint was rivet pull-out when the WC was greater than 30 kA. Similarly, the fracture mode of the Al/Cu joint obtained under the shorter welding time (200 ms) was the interfacial tearing, whereas the joint welded under a longer welding time (longer than 300 ms) presented the rivet pull-out fracture.

The nugget diameter, electrode indentation depth and interfacial microstructure not only affected the tensile shear load of the Al/Cu joint, but also determined the failure mode of the joint. Figure 8a,b show the schematic diagram of the joint fracture that presented interfacial tearing and rivet pull-out, respectively. The joints welded under the condition of lower WC or shorter WT not only had smaller nugget, but also the joining between the rivet shank and lower plate on the outside the nugget was weaker. Under the action of tensile load (F) and the resulting additional torque (M_T), the joint was first torn from the interface between the upper plate and lower plate (A and A′ location), and the failure crack propagated along the interface between the rivet shank and the lower plate, and then penetrated the nugget. Thus, the Al/Cu joint fractured as illustrated in Fig. 8a. When the larger welding current or longer welding time was utilized, the joint obtained not only had a larger nugget, and the joining between the rivet shank and lower plate outside the nugget was solid, but also had a deeper electrode indentation on its surface. Under the influence of the former, the forward propagation of the fracture crack during the tensile process of the joint was prevented at the B (B′) location as illustrated in Fig. 8b. The latter caused the lower plate thickness of the welding zone to become thinner. In the case, the fracture crack extended from the B (B′) location to the C (C′) location during the tensile process of the joint, which resulted in the rivet pull-out failure of the joint as illustrated in Fig. 8b. In addition, if the joining of the interface between the rivet shank and the upper plate was not achieved, the fracture crack would propagate along the interface (as shown by the green arrows in Fig. 8b) from the B (B′) location during the tensile process, which can also lead to the fracture of the joint. In this respect, the application of AG in the REW of Al/Cu can promote the joining between the rivet shank and the upper plate, thereby increase the tensile shear load of the Al/Cu joint.

It can be seen from above that the nugget diameter has a positive influence on the shear load of the Al/Cu joint and that the electrode indentation is the opposite. Therefore, the changing trend of tensile shear load of the Al/Cu joint with the WC and WT was considered to be a combined effect result of the nugget diameter and electrode indentation. In the range of 29–30 kA, or 200–400 ms, the influence of the nugget diameter on the
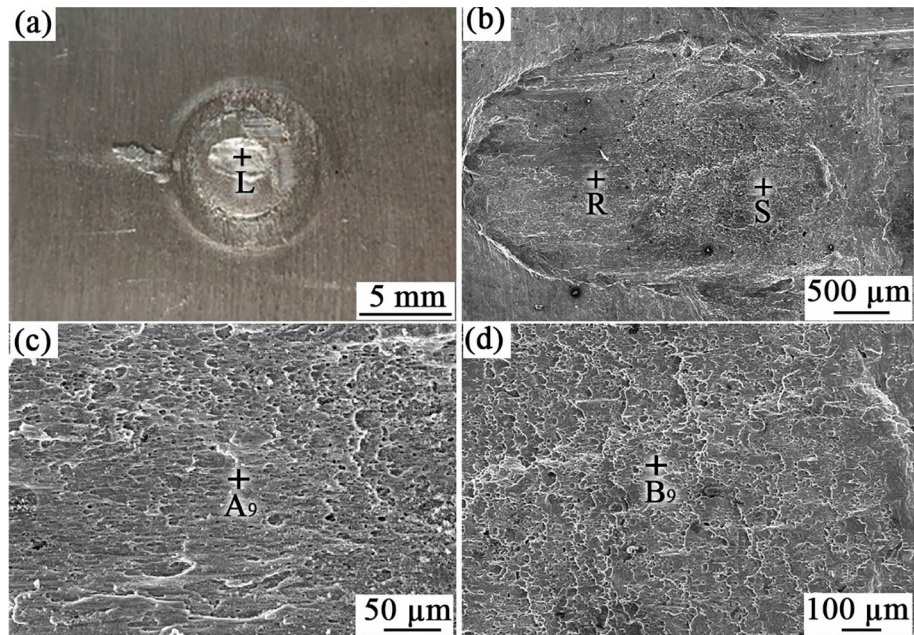
Fig. 9. Fracture of the Al/Cu joint (**a**) fracture macro appearance macrophotography at the lower side; (**b**) SEM image at the L location ; (**c**) enlarged SEM image of R zone; (**d**) enlarged SEM image of S zone.

tensile shear load of the Al/Cu joint was dominant. When the WC was larger than 30 kA or WT was longer than 400 ms, the effect of electrode indentation on the tensile shear load of the joint overrode that of the nugget diameter.

Figure 9a shows the lower plate side fracture of the Al/Cu joint that was fractured in interfacial tearing mode. The joint was welded under the conditions of 29 kA WC and 400 ms WT. Figure 9b demonstrates an enlarged SEM image at the L location in Fig. 9a. According to the morphology, the fracture may be divided into R and S regions. Figure 9c,d show enlarged images of parts of the R and S regions, respectively. The results of the composition analysis for the two regions (at A_9 and B_9 locations) are shown in Table 1. The EDS results reveal that the fracture of the Al/Cu joint occurred in aluminum as illustrated in Fig. 8a. Some dimples were observed in the fracture, which shows that the fracture of the joint presented certain toughness characteristics. The dimples in the R region were parabolic as shown in Fig. 9c, while those in the S region were not as shown in Fig. 9d. Due to the additional torque (M_T), the angle between the direction of the applied load and the normal direction of the tearing surface of the joint changed continuously during the tensile process. The fracture at the R zone mainly occurred when the applied load was parallel to the tearing surface of the joint, while the fracture in the S zone occurred when the two were nearly perpendicular.

Conclusion

In this study, A1060 rivet and AG were used to weld A1060 plate and T2 Cu plate in designed welding parameters. The main conclusions can be obtained as follows:

(1) A banded melting layer was formed in the aluminum adjacent to the upper plate when Al plate and Cu plate were welded by REW with AG of Ni

(2) A layer of Al_2Cu and the eutectic structure of Al_2Cu and (Al) were formed in the interfacial zone of Al/Cu when Al plate and Cu plate were welded by REW with AG of Ni.

(3) Nugget was composed of obvious orientation columnar crystal layers on the outer side and equiaxed crystals inside.

(4) With the increase of WC and the extension of WT, the tensile shear load of the Al/Cu joint increased first and then decreased. When the WC was 30 kA, the WT was 400 ms, the tensile shear load of the joint reached the maximum, approximately 2.55 kN.

Data availability

All data generated or analysed during this study are included in this published article.

References

1. Qiuchen, Ma., Cheng, S., Jianli, Z., Li, Z. & Hongjun, Ji. Dynamic Weld evolution during ultrasonic welding of Cu-Al joints. *Mater. Sci. Eng., A* **823**, 141724 (2021).

2. Kah, P., Vimalraj, C., Martikainen, J. & Suoranta, R. Factors influencing Al-Cu weld properties by intermetallic compound formation. *Int. J. Mech. Mater. Eng.* **10**, 10 (2015).
3. Mohsen, A., Mehrdad, K. & Yaser, V. Spot welding of Al-Cu sheets using the electromagnetic pulse for improving the quality of joints. *J. Adhes. Sci. Technol.* **36**(3), 261–286 (2022).
4. Bergmann, J. P., Regensburg, A., Schürer, R., Petzoldt, F. & Herb, A. Effect of the interface characteristics on the joint properties and diffusion mechanisms during ultrasonic metal welding of Al/Cu. *Weld. World* **61**(3), 499–506 (2017).
5. Renyi, Lu. et al. Composition design method of Al-Cu alloy for laser powder bed fusion. *J. Alloy. Compd.* **914**, 165298 (2022).
6. Li, F. S. et al. Investigation on the coupling interaction in electron beam welded Al–Cu bimetallic sheet. *Proc. Inst. Mech. Eng., Part L: J. Mater.: Des. Appl.* **235**(3), 640–652 (2021).
7. Uwe, R., Simon, O., Stefan, J. & Niklas, H. Influence of the degree of dilution with laser beam vacuum-welded Cu-Al mixed joints on the electrical properties. *Procedia CIRP* **74**, 23–26 (2018).
8. Udo, H., Alexander, I., Christoph, B., Jens, G. & Vesselin, M. Finite element modeling for the structural analysis of Al-Cu laser beam welding. *Phys. Procedia* **83**, 1404–1414 (2016).
9. Xue, Z., Hu, S., Shen, J., Zuo, D. & Kannatey-Asibu, E. Microstructure characterization and mechanical properties of laser-welded copper and aluminum lap joint. *J. Laser Appl.* **26**(1), 012002 (2014).
10. Wenqing, S., Wenhua, W. & Yanlu, H. Laser micro-welding of Cu-Al dissimilar metals. *Int. J. Adv. Manuf. Technol.* **85**(1–4), 185–189 (2016).
11. Mingshen, Li. et al. Friction stir spot welding of aluminum and copper: A review. *Materials* **13**(1), 156 (2020).
12. Zhou, L. et al. Effect of pin profile on microstructure and mechanical properties of friction stir spot welded Al-Cu dissimilar metals. *J. Manuf. Processes* **36**, 1–9 (2018).
13. Fujii, H. T., Endo, H., Sato, Y. S. & Kokawa, H. Interfacial microstructure evolution and weld formation during ultrasonic welding of Al alloy to Cu. *Mater. Charact.* **139**, 233–240 (2018).
14. Huan, Li., Biao, C., Jian, L. & Jingwei, Y. Modeling of high-power ultrasonic welding of Cu/Al joint. *Int. J. Adv. Manuf. Technol.* **97**, 833–844 (2018).
15. Mohammad, Z. & Majid, P. Metallurgical joining of aluminium and copper using resistance spot welding: Microstructure and mechanical properties. *Sci. Technol. Weld. Join.* **26**(6), 461–469 (2021).
16. Karim, M. A. et al. Critical effect of heat input on joint quality in resistance element welding of Al and steel. *J. Manuf. Processes* **95**, 91–104 (2023).
17. Yue, Y., Zhen, L., Yuanbo, Bi. & Yixuan, Z. Nano-scale characterization of intermetallic compounds in dissimilar aluminum-steel resistance element welded joints. *Mater. Charact.* **204**, 113227 (2023).
18. Zhanxiang, L. et al. Microstructure and fatigue behavior of resistance element welded dissimilar joints of DP780 dual-phase steel to 6061–T6 aluminum alloy. *Int. J. Adv. Manuf. Technol.* **92**(5–8), 1923–1931 (2017).
19. Manladan, S. M. et al. Resistance element weld-bonding and resistance spot weld-bonding of Mg alloy/austenitic stainless steel. *J. Manuf. Processes* **48**, 12–30 (2019).
20. Sizhe, N. et al. Resistance rivet welding of aluminum/titanium dissimilar materials. *J. Manuf. Processes* **108**, 141–152 (2023).
21. Zheng, B. et al. Microstructure and mechanical properties of Al/Mg resistance element welded joints. *Int. J. Adv. Manuf. Technol.* **120**(9–10), 6315–6323 (2022).
22. Qiu, R., Wang, N., Shi, H., Zhang, K. & Satonaka, S. Non-parametric effects on pore formation during resistance spot welding of magnesium alloy. *Sci. Technol. Weld. Join.* **19**(3), 231–234 (2014).
23. Tao, Ma. & Jing, T. Solidification morphology of Al-Cu alloy and its influencing factors. *Foundry Technol.* **32**(9), 1283–1286 (2011).

Author contributions

R.Q. and H.S. supervised the team activity. All authors contributed to the study's conception and design. Material preparation, data collection, and analysis were performed by D.C., J.W. and L.Y. The first draft of the manuscript was written by D.C. and all authors commented on previous versions of the manuscript. All authors read and approved the final manuscript.

Funding

Declarations

Competing interests

The authors declare no competing interests.

Additional information

Correspondence and requests for materials should be addressed to R.Q.

Reprints and permissions information is available at www.nature.com/reprints.

Publisher's note Springer Nature remains neutral with regard to jurisdictional claims in published maps and institutional affiliations.